Optically controllable THz chiral metamaterials

G. Kenanakis,[1,2,*] R. Zhao,[3] N. Katsarakis,[1,2] M. Kafesaki,[1,4] C. M. Soukoulis,[1,5] and E. N. Economou[1]

[1]*Institute of Electronic Structure and Laser, Foundation for Research & Technology-Hellas, P.O. Box 1385, Vassilika Vouton, 711 10 Heraklion, Crete, Greece*
[2]*Science Department, School of Applied Technology, Technological Educational Institute of Crete, 710 04 Heraklion, Crete, Greece*
[3]*The Blackett Laboratory, Department of Physics, Imperial College London, London SW7 2AZ, UK*
[4]*Department of Materials Science and Technology, University of Crete, 710 03 Heraklion, Crete, Greece*
[5]*Ames Laboratory-USDOE, and Department of Physics and Astronomy, Iowa State University, Ames, 50011 Iowa, USA*
[*]*gkenanak@iesl.forth.gr*

Abstract: Switchable and tunable chiral metamaterial response is numerically demonstrated here in different uniaxial chiral metamaterial structures operating in the THz regime. The structures are based on the bi-layer conductor design and the tunable/switchable response is achieved by replacing parts of the metallic components of the structures by photoconducting Si, which can be transformed from an insulating to an almost conducting state through photoexcitation, achievable under external optical pumping. All the structures proposed and discussed here exhibit frequency regions with giant tunable circular dichroism, as well as regions with giant tunable optical activity, showing unique potential in the achievement of active THz polarization components, like tunable polarizers and polarization filters.

OCIS codes: (160.3918) Metamaterials; (160.5140) Photoconductive materials; (160.1585) Chiral media.

References and links

1. M. Wegener and S. Linden, "Giving light yet another new twist," Physics **2**, 3–6 (2009).
2. J. K. Gansel, M. Thiel, M. S. Rill, M. Decker, K. Bade, V. Saile, G. von Freymann, S. Linden, and M. Wegener, "Gold Helix Photonic Metamaterial as Broadband Circular Polarizer," Science **325**(5947), 1513–1515 (2009).
3. K. Murata, M. Aoki, T. Suzuki, T. Harada, H. Kawabata, T. Komori, F. Ohseto, K. Ueda, and S. Shinkai, "Thermal and Light Control of the Sol-Gel Phase Transition in Cholesterol-Based Organic Gels. Novel Helical Aggregation Modes As Detected by Circular Dichroism and Electron Microscopic Observation," J. Am. Chem. Soc. **116**(15), 6664–6676 (1994).
4. N. Koumura, R. W. J. Zijlstra, R. A. van Delden, N. Harada, and B. L. Feringa, "Light-driven monodirectional molecular rotor," Nature **401**(6749), 152–155 (1999).
5. J. J. D. de Jong, L. N. Lucas, R. M. Kellogg, J. H. van Esch, and B. L. Feringa, "Reversible Optical Transcription of Supramolecular Chirality into Molecular Chirality," Science **304**(5668), 278–281 (2004).
6. K. Ikeda, W. Liu, Y. R. Shen, H. Uekusa, Y. Ohashi, and S. Y. Koshihara, "Photo-induced chirality switching in a cobaloxime complex crystal," J. Chem. Phys. **122**(14), 141103 (2005).
7. S. Zhang, J. Zhou, Y. S. Park, J. Rho, R. Singh, S. Nam, A. K. Azad, H. T. Chen, X. Yin, A. J. Taylor, and X. Zhang, "Photoinduced handedness switching in terahertz chiral metamolecules," Nat. Commun. **3**, 942 (2012).
8. J. Zhou, D. R. Chowdhury, R. Zhao, A. K. Azad, H. Chen, C. M. Soukoulis, A. J. Taylor, and J. F. O'Hara, "Terahertz chiral metamaterials with giant and dynamically tunable optical activity," Phys. Rev. B **86**(3), 035448 (2012).
9. B. Wang, J. Zhou, Th. Koschny, M. Kafesaki, and C. M. Soukoulis, "Chiral metamaterials: simulations and experiments," J. Opt. A, Pure Appl. Opt. **11**(11), 114003 (2009).
10. E. Plum, J. Zhou, J. Dong, V. A. Fedotov, T. Koschny, C. M. Soukoulis, and N. I. Zheludev, "Metamaterial with negative index due to chirality," Phys. Rev. B **79**(3), 035407 (2009).
11. Z. Li, K. B. Alici, H. Caglayan, M. Kafesaki, C. M. Soukoulis, and E. Ozbay, "Composite chiral metamaterials with negative refractive index and high values of the figure of merit," Opt. Express **20**(6), 6146–6156 (2012).
12. G. Kenanakis, R. Zhao, A. Stavrinidis, G. Konstantinidis, N. Katsarakis, M. Kafesaki, C. M. Soukoulis, and E. N. Economou, "Flexible chiral metamaterials in the terahertz regime: a comparative study of various designs," Opt. Mater. Express **2**(12), 1702–1712 (2012).
13. J. Zhou, J. Dong, B. Wang, Th. Koschny, M. Kafesaki, and C. M. Soukoulis, "Negative refractive index due to chirality," Phys. Rev. B **79**(12), 121104 (2009).

#203516 - $15.00 USD Received 20 Dec 2013; revised 7 Mar 2014; accepted 23 Mar 2014; published 13 May 2014

14. M. Decker, M. Ruther, C. E. Kriegler, J. Zhou, C. M. Soukoulis, S. Linden, and M. Wegener, "Strong optical activity from twisted-cross photonic metamaterials," Opt. Lett. **34**(16), 2501–2503 (2009).
15. Z. Li, M. Mutlu, and E. Ozbay, "Chiral metamaterials: from optical activity and negative refractive index to asymmetric transmission," J. Opt. **15**(2), 023001 (2013).
16. X. Xiong, W. H. Sun, Y. J. Bao, M. Wang, R. W. Peng, C. Sun, X. Lu, J. Shao, Z. F. Li, and N. B. Ming, "Construction of a chiral metamaterial with a U-shaped resonator assembly," Phys. Rev. B **81**(7), 075119 (2010).
17. R. Zhao, L. Zhang, J. Zhou, Th. Koschny, and C. M. Soukoulis, "Conjugated gammadion chiral metamaterial with uniaxial optical activity and negative refractive index," Phys. Rev. B **83**(3), 035105 (2011).
18. D. H. Kwon, P. L. Werner, and D. H. Werner, "Optical planar chiral metamaterial designs for strong circular dichroism and polarization rotation," Opt. Express **16**(16), 11802–11807 (2008).
19. M. Kafesaki, N. H. Shen, S. Tzortzakis, and C. M. Soukoulis, "Optically switchable and tunable terahertz metamaterials through photoconductivity," J. Opt. **14**(11), 114008 (2012).
20. N. H. Shen, M. Massaouti, M. Gokkavas, J. M. Manceau, E. Ozbay, M. Kafesaki, Th. Koschny, S. Tzortzakis, and C. M. Soukoulis, "Optically Implemented Broadband Blueshift Switch in the Terahertz Regime," Phys. Rev. Lett. **106**(3), 037403 (2011).
21. M. Decker, M. W. Klein, M. Wegener, and S. Linden, "Circular dichroism of planar chiral magnetic metamaterials," Opt. Lett. **32**(7), 856–858 (2007).
22. D. H. Kwon, P. L. Werner, and D. H. Werner, "Optical planar chiral metamaterial designs for strong circular dichroism and polarization rotation," Opt. Express **16**(16), 11802–11807 (2008).
23. J. Gu, R. Singh, A. K. Azad, J. Han, A. J. Taylor, J. F. O'Hara, and W. Zhang, "An active hybrid plasmonic metamaterial," Opt. Mater. Express **2**(1), 31 (2012).
24. H. T. Chen, J. F. O'Hara, A. K. Azad, A. J. Taylor, R. D. Averitt, D. B. Shrekenhamer, and W. J. Padilla, "Experimental demonstration of frequency-agile terahertz metamaterials," Nat. Photonics **2**(5), 295–298 (2008).
25. B. Wang, J. Zhou, T. Koschny, and C. M. Soukoulis, "Nonplanar chiral metamaterials with negative index," Appl. Phys. Lett. **94**(15), 151112 (2009).
26. U. Fano, "Effects of Configuration Interaction on Intensities and Phase Shifts," Phys. Rev. **124**(6), 1866–1878 (1961).
27. Z. Li, K. B. Alici, E. Colak, and E. Ozbay, "Complementary chiral metamaterials with giant optical activity and negative refractive index," Appl. Phys. Lett. **98**(16), 161907 (2011).
28. X. J. He, Y. Wang, Z. X. Geng, J. M. Wang, and T. L. Gui, "3D broadband isotropic NRI metamaterial based on metallic cross-pairs," J. Magn. Magn. Mater. **323**(20), 2425–2428 (2011).
29. M. Decker, R. Zhao, C. M. Soukoulis, S. Linden, and M. Wegener, "Twisted split-ring-resonator photonic metamaterial with huge optical activity," Opt. Lett. **35**(10), 1593–1595 (2010).
30. J. D. Jackson, *Classical Electrodynamics*, 3rd ed. (Wiley, 1998).

1. Introduction

Metamaterials, i.e. composite structured materials with novel and unique electromagnetic properties, unattainable in natural materials, attract more and more increasing attention. Metamaterial properties like negative magnetic permeability, negative refractive index, refractive index close to zero, hyperbolic dispersion relation, empower metamaterials with unique possibilities for the control of electromagnetic waves. A particularly interesting category of metamaterials is that of chiral metamaterials, as they offer great possibilities in the control of the light polarization [1–8]. In chiral metamaterials optical activity (i.e. polarization rotation of a linearly polarized wave) and circular dichroism (i.e. the absorption difference between left- and right-handed circularly polarized light) can exceed the corresponding effects in natural chiral materials by many orders of magnitude. Moreover, chiral metamaterials offer a path for the achievement of negative refractive index and all the novel and unique properties and capabilities associated with negative index metamaterials.

Although the study of macroscopic chiral structures is a long-term and well-established topic in microwave engineering, recently a new category of chiral structures was demonstrated in the framework of the metamaterials research, and gave the possibility to extend the concepts and results regarding chiral structures to higher frequencies, all the way up to optical regime. These are planar structures based on a pair of conductors which are not electrically but electromagnetically coupled, with this electromagnetic coupling being the source of the chiral response. Many such structures have been recently proposed, like pairs of rossetes [9–11] or crosses [9,12–14], mutually twisted to create chirality, chiral designs based on U-shaped SRRs [15,16] or on gammadion structures [8,12,17,18], etc. Since this type of paired conductor structures are planar structures, they can be easily fabricated with planar technologies and can be scaled from mm to nm scale, giving chiral metamaterials operating from microwaves up to the optical regime. All these structures have exhibited large chiral

#203516 - $15.00 USD Received 20 Dec 2013; revised 7 Mar 2014; accepted 23 Mar 2014; published 13 May 2014

response, translated to giant optical activity and/or very large circular dichroism and/or negative index of refraction for either left- or right-handed circular polarization, in various frequency regimes. These properties show the unambiguous potential of the paired-conductor structures to create effective polarization control components, like polarization filters and polarizers, particularly important in the THz regime where there is a serious lack of optical components.

Despite the large amount of work on passive chiral metamaterials of the paired-conductor type, there is serious lack of work regarding tunable and switchable chirality, which would allow dynamic control of the polarization of light and will find important applications, especially in manipulation of THz waves, as it will offer means to create dynamical components, like wave-plates, modulators, dynamical filters and polarizers. Recently a tunable/switchable chiral such metamaterial was proposed and demonstrated in the THz regime [7,8], where the chirality switch was based on the photoexcitation of the metamaterial substrate. Employing a photoconductive substrate as a means to create switchable metamaterials is one of the main ways proposed so-far to switch the various metamaterial properties [19]. This way though does not selectively "act" at specific metamaterial frequency regimes but rather changes all the spectrum of the metamaterial response, resulting to almost zero transmission at the case of large substrate photoconductivity.

Another way to use photoconductive material to achieve tunable or switchable response is to insert it properly in the metallic components of the metamaterial structure, as to selectively and at will affect specific metamaterial resonances. This approach has been already succeeded, e.g., to give blue-shift tunability and dual-band switch in electrically-driven split-ring resonator-based systems [20]. Here we apply the same approach to demonstrate tunable and switchable chiral response.

More specifically, we numerically demonstrate very large tunable optical activity and switchable ellipticity response in different chiral metamaterial structures operating in the THz regime, by properly inserting into the structures photoconducting silicon, which can be transformed from an insulating to a conducting state by photoexcitation. The all-metal version of our structures (i.e. with no Si) and with the same geometrical parameters as discussed here, have been already investigated, both theoretically and experimentally [12], and have shown quite large pure optical activity response and negative refractive index for both left-handed and right-handed circularly polarized waves. Moreover, since they are planar designs they can be easily fabricated using UV lithography, as reported in [12], and they can be fully flexible. We start our discussion here by presenting the designs, along with the description of our investigation approach (section 2), and we continue with the presentation of transmission results, from which we extract the chiral response of the structures (section 3). In section 4 we present a dual form of our structures, inspired by the complementary Babinet's principle, and we discuss their switchable/tunable chiral response. We finish with our conclusions and perspectives.

2. The structures and investigation approach

The basic chiral designs employed in the present study are introduced in Fig. 1, while their geometrical features are presented in Table 1. The unit cell of the first design [see Figs. 1(a) and 1(b)] is composed of a pair of crosses *(cross-wires design)* rotated against each other by an angle of $\varphi = 30°$. The back cross is made entirely of metal (considered here as silver – see yellow color in Fig. 1), while in the front cross parts of the silver have been replaced by photoconducting Si (gray color in Fig. 1). The cross-pair design, with both crosses made of metal, was first studied in GHz range [13], where it showed a pure optical activity as high as 448° per wavelength (at 7 GHz) and negative index of refraction, and subsequently in the optical regime [14], showing optical activity around 62° per wavelength (at 220 THz) but no negative index. Recently the design was studied also in the THz regime [12] (with the same structure parameters as the ones considered here) where it showed optical activity as high as 257° per wavelength at 5.8 THz, associated with 40% transmission. Here, we study the effect

#203516 - $15.00 USD Received 20 Dec 2013; revised 7 Mar 2014; accepted 23 Mar 2014; published 13 May 2014

of replacing parts of the silver by photoconductive Si, as shown in Figs. 1(a) and 1(b), and the resulting possibility of tuning the optical response of the structure by external illumination.

Our second design is based on the conjugated gammadion structure [17] and consists of a pair of silver crosses with Z-type arms, as shown in Fig. 1(c), where parts of the silver in the front Z-cross have been replaced by Si (grey color in Fig. 1). The conjugated gammadion design was studied recently in the microwave regime, where two resonant modes have been identified, one predominantly magnetic and the other predominantly electric, giving negative index of refraction for either left-handed or right-handed circularly polarized waves [17]. Moreover, the Z-shaped structure was studied both theoretically and experimentally in the far-infrared [12] and the near-infrared/visible region [21,22] exhibiting strong circular dichroism and polarization rotation.

In all our designs the conjugated arrangement of the metallic resonators is such as to lead to no center of inversion and no mirror-symmetry plane for the structure, which, in combination with the C_4 rotational symmetry of all the designs [17], ensures pure chiral response, i.e. that the eigenmodes in all cases are pure circularly polarized waves.

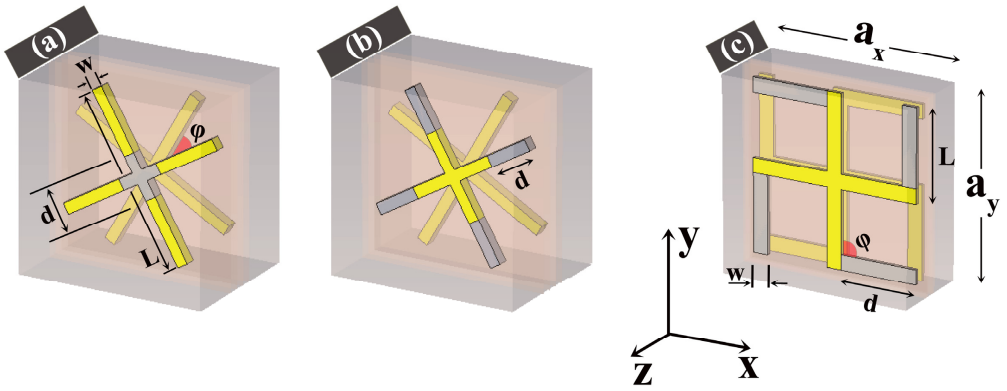

Fig. 1. Schematic of the unit cell of the chiral metamaterials under consideration: (a), (b) cross-wires and (c) Z-type crosses with φ = 90°, respectively. Grey color corresponds to photoconductive silicon and yellow corresponds to metal (silver). The metal (yellow-color) thickness t_m and the dimensions a_x, a_y, L, w, d and φ, for each design are presented in Table 1. The wave propagation is along the z direction.

Table 1. Dimensions (in Microns) of Chiral Metamaterials under Consideration (See Fig. 1).

Chiral metamaterial	a_x	a_y	t_m	L	w	d	φ
Cross-wires, Fig. 1(a) and Fig. 1(b)	17.0	17.0	1.0	16.0	1	4	30
Z-type crosses with φ = 90°, Fig. 1(c)	26.0	26.0	0.5	14.5	2.0	12.5	90

As can be seen in Fig. 1, our structures are planar and based on the bi-layer conductor configuration, where the chiral response results from electromagnetic coupling between the two properly shaped or oriented layers of conducting elements. The design of the structures is based on alternating polyimide (with a dielectric constant of 2.9) and silver, embedded in polyimide. In all the designs the sequence of layers starts with a 5 μm thick layer of polyimide. A silver structure (with a thickness t_m of 0.5 or 1.0 μm, depending on the design) is grown on top and another layer of polyimide (spacer layer, with a thickness of 1 μm (from metal to metal)) is built next. On top of it the combined metal-semiconductor structure is placed (see Fig. 1 for details), while the sequencing of layers ends with another 5 μm thick polyimide layer. This kind of layer-by-layer structures can be easily fabricated using UV-lithography as is reported in [12].

To calculate and analyze the response of our structures we have performed full-wave transmission and reflection simulations, using a commercial three-dimensional full-wave

#203516 - $15.00 USD Received 20 Dec 2013; revised 7 Mar 2014; accepted 23 Mar 2014; published 13 May 2014

solver (CST Microwave Studio) based on the Finite Integration Technique. For each chiral design we have considered in the simulations a single unit cell, as shown in Fig. 1, with *z*-direction being the propagation direction and periodic boundary conditions along *x* and *y* directions. For the metallic parts (silver; yellow color in Fig. 1) of the metamaterials we have considered a lossy-metal model with a conductivity of $\sigma_{Ag} = 6.3 \times 10^7$ S/m. For the photoactive silicon areas (marked in grey in Fig. 1 and with geometrical features mentioned in Table 1) which replace parts of the metal of the front metal-layer, we applied a simple conductivity model, considering $\varepsilon_{Si} = 11.9$, and conductivity, σ_{Si}, varying from 2.5×10^{-4} S/m (corresponding to no illumination, i.e. insulating Si) to 1×10^5 S/m, which is the maximum recorded conductivity achieved experimentally by means of optical pumping, using a 30-fs laser system at 800 nm central wavelength [8,19,20,23,24] (More specifically, as concluded in Ref [24], pump power of 500 mW, which is a quite large power for today's laser-systems, results to $\sigma_{Si} = 50000$ S/m).

3. Results and discussion

Before examining the dynamic response of the designs under consideration, we studied, for reference, the full metallic case in which the structures consist of only silver and polyimide. Then we considered the cases with Si replacing parts of the metal as shown in Fig. 1 and noted in Table 1. Especially for the cross-wires design we studied two different cases for the photoconductive silicon configuration: a) Si in the center of the structure [see Fig. 1(a) and 1(b)] Si at the edges of the structure [see Fig. 1(b)]. For the Z-type crosses, we have studied the case of Silicon in the arms of the structure [see Fig. 1(c)].

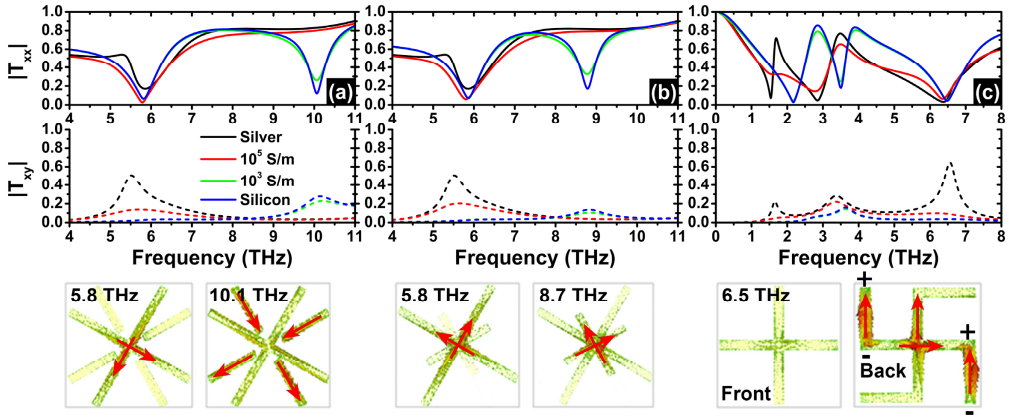

Fig. 2. Simulated transmission amplitudes $|T_{xx}|$ (upper panels) and $|T_{xy}|$ (lower panels), for the chiral metamaterials shown in Fig. 1, for linearly polarized incident wave. One can see the cases of Silver (black lines) and photoconductive Silicon with $\sigma_{Si} = 1 \times 10^5$ S/m (red lines) or 1×10^3 S/m (green lines) or 2.5×10^{-4} S/m (blue lines), respectively. The insets show the corresponding current distributions at the resonance frequencies for $\sigma_{Si} = 1 \times 10^3$ S/m with the E_y linearly polarized incident wave.

Our analysis of the response of the structure starts with calculation of the transmission for linearly polarized incident wave. This calculation provides a first assessment of the optical activity response of the structures and offers the possibility of a direct comparison with any future experiment, where the quantities that are usually measured are the transmission amplitudes for linearly polarized waves. To fully analyze and quantify the structures response, especially in what concerns dichroic response, we calculate the transmission amplitudes for circularly polarized incident waves (through the linear transmission data), from which we extract the ellipticity and the optical activity of the transmitted light, determining thus the polarization control properties and capabilities of our structures.

#203516 - $15.00 USD Received 20 Dec 2013; revised 7 Mar 2014; accepted 23 Mar 2014; published 13 May 2014

3.1 Transmission for linearly polarized incident wave

In Fig. 2 [panels (a) (b), (c)] we show the simulated transmission amplitudes $|T_{xx}|$ (upper panels in Fig. 2) and $|T_{xy}|$ (lower panels in Fig. 2) for the designs of Fig. 1 (panels (a), (b) and (c) respectively), for the cases of only silver (black lines) and of photoconductive silicon with $\sigma_{Si} = 1 \times 10^5$ S/m (red lines), 1×10^3 S/m (green lines), 2.5×10^{-4} S/m (blue lines). The simulated data are for linearly polarized fields, thus, in principle, four transmission components, T_{xx}, T_{xy}, T_{yx} and T_{yy}, can be calculated, where the first and second indices indicate the output and input signal polarizations, respectively, e.g. $T_{xy} = E_x^t / E_y^i$, where E_y^i is the input y-polarized electric field and E_x^t is the transmitted x-polarized electric field [25]. Due to the four-fold rotational symmetry of our structures $T_{xx} = T_{yy}$ and $T_{xy} = -T_{yx}$, so only two transmission amplitudes, e.g. T_{xx} and T_{xy}, are needed to be considered.

In Fig. 2(a) one should notice that the transmission amplitudes $|T_{xx}|$ (solid lines) and $|T_{xy}|$ (dashed lines) for the cross-wires structure where both crosses are made by silver are the same as the ones shown in [12], with a Fano-type resonance [26] at ~5.5 THz arising from the overlap of a magnetic-like resonance (associated with "antiparallel" currents between the crosses) and a broader electric-like resonance (associated with "parallel" currents between the crosses). These two resonances result from the coupling of the two dipole-like resonances of the two individual crosses [27,28]. If we gradually reduce the conductivity in the middle-part of the front cross (by replacing Silver with Si), the two crosses will become significantly different and the coupling between them will be substantially changed, leading to the disappearance of the magnetic-like resonance observed at ~5.5 THz in the pure metal case, while the electric dipole-like resonance (at around the same frequency) remains almost unchanged, as it is not strongly affected by the coupling between the crosses and it is supported now by the back-cross; we also observe the emergence of a second resonance coming from the dipole-like response of the metallic parts of the top broken-cross. It appears at higher frequencies due to the shorter length of these metallic parts compared to the full-cross. The above mentioned origin of the resonances is supported by the insets of Fig. 2(a) showing the current at the two resonances observed for $\sigma_{Si} = 1 \times 10^3$ S/m. At the first resonance the current is mainly distributed on the back cross. At the second resonance the current at the broken-cross is much larger than that on the full-cross; in this case the external field drives the whole resonator through the short wires of the broken-cross. It is worth-noticing here that the conductivity value $\sigma_{Si} = 1 \times 10^5$ S/m, is not high enough to establish a conducting behavior for Si (as can be concluded by comparing the red curves of Fig. 2 with the black curves which describe the all-metal case), leading to a magnetic-like response of the Si-incorporating structure.

The same behavior as in Fig. 2(a) is observed in the case of Fig. 2(b). Decreasing the conductivity, the front-cross gradually becomes a mini-one. The original Fano-like resonance observed in the full-metal case disappears since the coupling between these two discrepant crosses becomes weak. Meanwhile, a new clean resonance develops at ~8.8 THz corresponding to the dipole-like resonance of the front mini-cross. These two resonances eventually are unrelated and supported by the mini- and full- crosses respectively. The current distributions for each resonance for $\sigma_{Si} = 1 \times 10^3$ S/m are shown in the insets in Fig. 2(b). At each resonance frequency, only one of the crosses is strongly excited.

In Fig. 2(c) one can see the $|T_{xx}|$ and $|T_{xy}|$ transmission coefficients for the Z-type structure in which silicon is placed in the arms of the front design [see Fig. 1(c)]. As can be observed in Fig. 2(c), reducing the conductivity in the grey parts from the silver value (black lines) to 1×10^5 S/m (red lines) one can see first the weakening of the lower-frequency resonance of the structure (around 1.5 THz) which is mainly magnetic in origin. Reducing further the conductivity the electric resonance of the structure (at ~3THz) splits into two resonances, corresponding to the dipole-like resonance of the front and back structure. The third resonance around 6.5 THz corresponds to the octupole-like resonance as shown in the inset of Fig. 2(c), where the bended arms are strongly coupled to the external field and drive the

#203516 - $15.00 USD Received 20 Dec 2013; revised 7 Mar 2014; accepted 23 Mar 2014; published 13 May 2014

resonance of the whole structure. This resonance is almost not affected in position by the conductivity of the grey areas of the inset because the grey area is coincidently a "petal" of the octupole-like resonator. However, the amplitude of $|T_{xy}|$ changes a lot when the conductivity changes from the silver value to 1×10^5 S/m, because for the Silver, the two identical resonators at back and front side resonate out of phase coherently. When the conductivity changes to 1×10^5 S/m, the identity is broken. The system is essentially changed to be not in phase. The large amplitude gives a strong chirality at this frequency.

3.2 Response to circularly polarized incident wave

In order to quantify the optical activity of our structures and analyze their capabilities to create dynamic polarization manipulation components, one needs to study and analyze the transmission results for circularly polarized waves. These results can be directly calculated from the linearly polarized transmission data [13] according to the equation:

$$\begin{pmatrix} T_{++} & T_{+-} \\ T_{-+} & T_{--} \end{pmatrix} = \frac{1}{2} \times \begin{pmatrix} \left(T_{xx} + T_{yy}\right) + i\left(T_{xy} - T_{yx}\right) & \left(T_{xx} - T_{yy}\right) - i\left(T_{xy} + T_{yx}\right) \\ \left(T_{xx} - T_{yy}\right) + i\left(T_{xy} + T_{yx}\right) & \left(T_{xx} + T_{yy}\right) - i\left(T_{xy} - T_{yx}\right) \end{pmatrix} \quad (1)$$

which for bi-isotropic chiral structures can be simplified to $T_{++} = T_{xx} + iT_{xy}$, $T_{-} = T_{xx}$-iT_{xy}, T_{+-} $= T_{-+} = 0$. In the above relations the subscript + denotes the right-handed circularly polarized wave (RCP, +) and the subscript – the left-handed circularly polarized wave (LCP, –), while the first subscrtipt again denotes the polarization of the transmitted wave and the second the polarization of the incident wave.

The transmission amplitudes for circularly polarized waves, T_{++} and T_{--} (obtained through Eq. (1)), for all our chiral structures, as the conductivity of silicon part is decreased from the silver value of $\sigma_{Ag} = 6.3 \times 10^7$ S/m all the way to 2.5×10^{-4} S/m, are shown in Fig. 3. The cross polarized transmissions T_{-+} and T_{+-} are negligible, as expected since our structures are bi-isotropic chiral structures,and, therefore, not shown here.

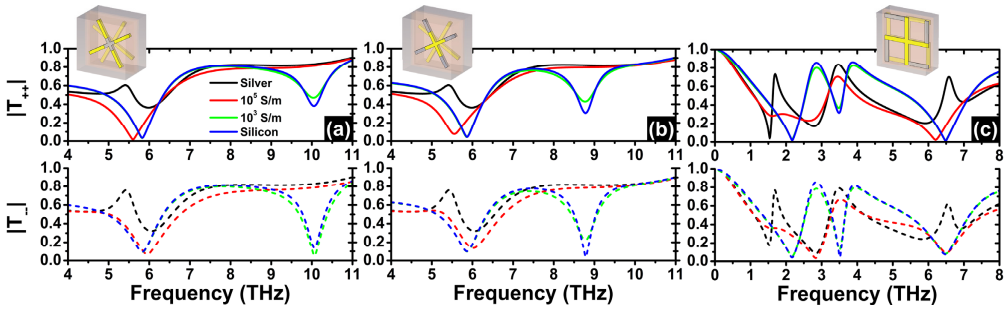

Fig. 3. Simulated magnitude of the transmission coefficients for the right circularly polarized, $|T_{++}|$ (solid lines), and the left circularly polarized, $|T_{--}|$ (dashed lines), electromagnetic wave, for the chiral metamaterials under consideration. One can see the cases of Silver (black lines) and photoconductive Silicon with $\sigma_{Si} = 1 \times 10^5$ S/m (red lines) to 1×10^3 S/m (green lines) and 2.5×10^{-4} S/m (blue lines), respectively. The insets show the corresponding designs in which grey color corresponds to photoconductive Silicon and yellow corresponds to metal (Silver).

The most pronounced feature observed in Fig. 3 is the various switchable transmission regimes for all structures, where by changing the Si conductivity from the insulating value to 10^5 the transmission amplitude changes by more than 80%.

Besides that switchable transmission, one worth-noticing feature in the cross-wires structure is that by reducing the conductivity from the silver value to 10^5 S/m the transmission dip for left-handed circularly polarized wave (at ~6 THz) appears at slightly higher frequencies than that of the right-handed wave. Reducing further the Si conductivity the *T*-dips for the two polarizations coincide again in frequency. This peculiar non-monotonic response, which suggest strong circular dichroism (defined as $|T_{++}|^2$-$|T_{--}|^2$) appears in the cases

#203516 - $15.00 USD Received 20 Dec 2013; revised 7 Mar 2014; accepted 23 Mar 2014; published 13 May 2014

that Si responds mainly as lossy material. The same non-monotonic response is observed also for the Z-cross structure at around 6.2 to 6.5 THz. In both cases this response seems to be a feature appearing as a first step of the disappearance (by decreasing σ_{Si}) of a Fano-type resonance due to the coupling of electric-dipole and magnetic resonance of the paired-conductor structure. This observation possibly suggests that by increasing the conductivity of Si from the insulator value to that of the almost metallic one the magnetic coupling between the paired "conductors" develops at an earlier stage (i.e. requires lower conductivity) for one of the two circular polarizations, depending on the structure helicity.

To quantify the dichroic response and the dynamical polarization control capabilities of our structures, we elaborated further on the transmission results, calculating the polarization azimuth rotation angle and the ellipticity of the transmitted wave. The polarization azimuth rotation angle θ (for a linearly polarized incident wave θ is the angle between the major ellipse axis of the elliptically polarized transmitted wave and the polarization of the incident wave), indicative of the optical activity of the structures, can be calculated as $\theta = [\arg(T_{++}) - \arg(T_{--})]/2$ [9,29,30], while the ellipticity η of the transmitted wave is defined as $\eta = \sin^{-1}[(|T_{++}|^2 - |T_{--}|^2)/(|T_{++}|^2 + |T_{--}|^2)]/2$ [9,29,30] (zero η corresponds to linearly polarized transmitted wave, while 45° corresponds to right-handed circularly polarized wave (RCP) and –45° to left-handed circularly polarized wave (LCP); intermediate values indicate elliptically polarized wave).

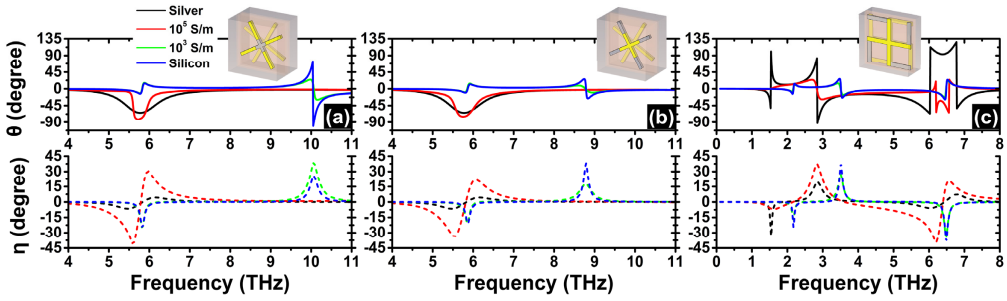

Fig. 4. Simulated azimuth rotation angle, θ (solid lines) and simulated ellipticity, η (dashed lines), for the chiral metamaterials under consideration. One can see the cases of Silver (black lines) and photoconductive Silicon with $\sigma_{Si} = 1 \times 10^5$ S/m (red lines) or 1×10^3 S/m (green lines) or 2.5×10^{-4} S/m (blue lines), respectively. The insets show the corresponding designs in which grey color corresponds to photoconductive Silicon and yellow corresponds to metal (Silver). Note that the sharp peaks and jumps in the rotation angle are a result of the strong resonant response.

The simulated azimuth rotation angle, θ, and the ellipticity, η, for each of the chiral structures shown in Fig. 1 are shown in Fig. 4, for different values of the Si conductivity.

Figure 4 clearly demonstrates the notable switchable polarizer capabilities of our structures in various frequency regimes: Regarding the cross-wires structure around 5.5 THz, it can be easily switched from circular to linear polarizer by changing the flux of the excitation power. Similar switchable response is observed also at ~10 THz for the cross-structure of Fig. 1(a) and at ~8.8 THz for the cross-structure of Fig. 1(b). The same switchable polarizer response is observed also for the Z-cross structure at the frequencies around 3 THz and 6.2 THz.

Examining in detail the ellipticity features presented in Fig. 4, one can conclude that regardless of the position or the size of silicon parts, for every chiral design presented in Fig. 1, there is an optimum conductivity ($\sigma_{Si} = 1 \times 10^5$ S/m) which produces an impressive maximum ellipticity reaching almost ± 45 degrees (~100% transformation of an incoming linearly polarized into a circularly polarized transmitted wave). To demonstrate this more clearly, in Fig. 5 we plotted the maximum values of ellipticity *(η)* for the cross-wires design with silicon in the center of the structure as a function of the conductivity σ_{Si}, in the frequency range 5-7 THz. Figure 5 shows the non-monotonic response of the ellipticity of the

#203516 - $15.00 USD Received 20 Dec 2013; revised 7 Mar 2014; accepted 23 Mar 2014; published 13 May 2014

transmitted wave as a function of the Si conductivity, demonstrating maximum ellipticity for $\sigma_{Si} = 10^5$ S/m. As we have already discussed in connection with Fig. 3, the origin of this large ellipticity is the slight shift of the lower-frequency structure resonance for LCP waves compared to that for RCP waves.

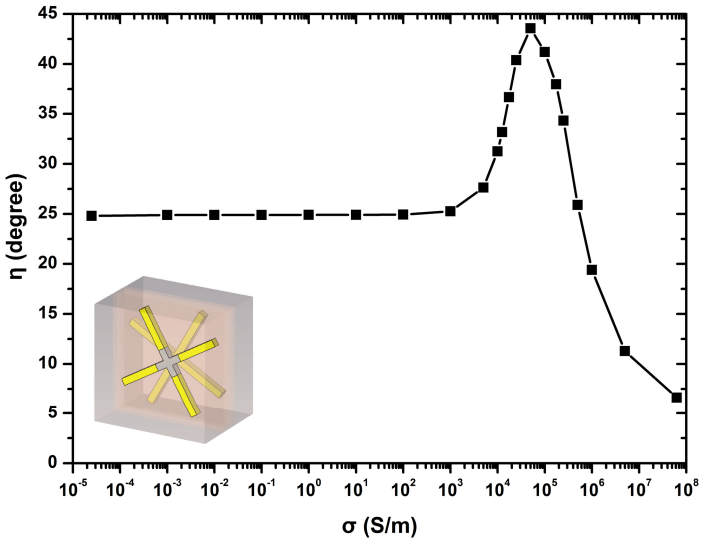

Fig. 5. Impressive variation of the simulated maximum ellipticity, η, for the cross-wires design with Silicon in the center of the structure as a function of photoconductivity σ_{Si}, in the frequency range 5-7 THz.

Examining the polarization azimuth rotation angle shown in Fig. 4, we can observe for the optical activity of our structures the same impressive dynamical tuning as mentioned above for the ellipticity. For the cross-pair design the optical activity at ~5.7 THz (where ellipticity is close to zero) can be tuned from ~90 to ~10 degrees by changing the excitation power. Similarly large tunable optical activity response is observed for the Z-cross structure around 6.4 THz, with considerable optical activity tuning in other frequency regimes too.

4. Complementary structures

Prompted by the impressive dynamic polarization control capabilities of our designs in connection with the analogies in the scattering response between Babinet's complementary screens, we investigated also a complementary-like form of our designs, where each conductor layer of the bi-layer structure is replaced by its complementary layer, i.e. in the layers where the metal structures was previously imprinted now metal and dielectric (polyimide) are exchanged. Such types of chiral structures have been already studied in the literature [27], showing large optical activity response associated with very high transmittance.

Here, to achieve dynamic response from our "complementary" structures, we additionally replaced the front metal layer by photoconducting Si (see insets in Fig. 6), and we examined the response of the structures as the Si conductivity changed from 10^5 S/m (corresponding to the maximum conductivity achievable under optical pumping) to 2.5×10^{-4} S/m (corresponding to pure insulating Si).

The response of the resulting structures (including the pure metal, i.e. no Si, case) regarding transmission for linearly polarized incident wave, for circularly polarized incident wave as well as ellipticity and optical activity are shown Fig. 6.

#203516 - $15.00 USD Received 20 Dec 2013; revised 7 Mar 2014; accepted 23 Mar 2014; published 13 May 2014

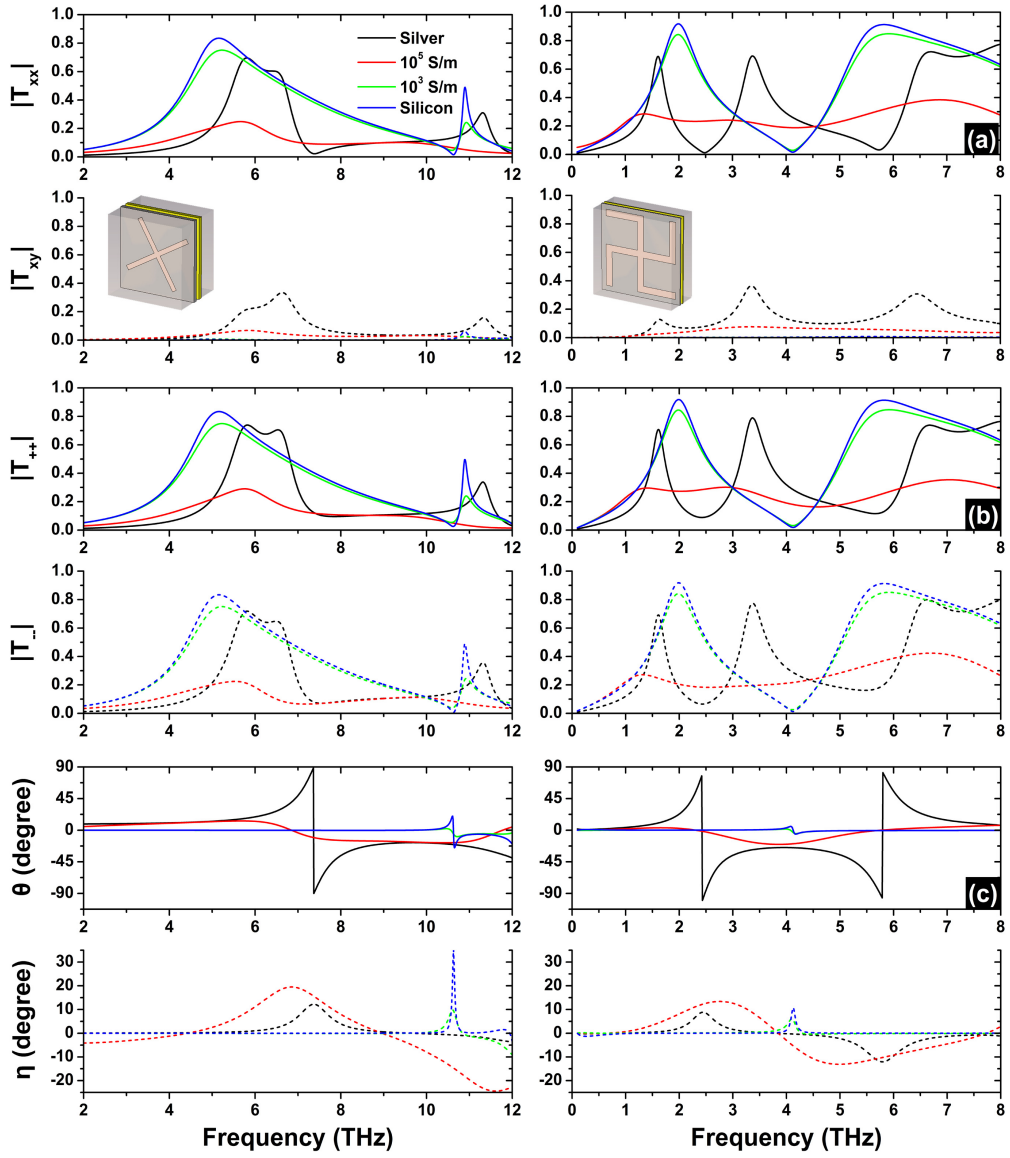

Fig. 6. (a) Each column shows the simulated transmission amplitudes for linearly polarized incident wave $|T_{xx}|$ (solid lines) and $|T_{xy}|$ (dashed lines) for the structure shown in the inset, (b) the transmission amplitudes for circularly polarized incident waves $|T_{++}|$ (solid lines) and $|T_{--}|$ (dashed lines), and (c) the azimuth rotation angle, θ (solid lines) and the ellipticity, η (dashed lines). One can see the cases where the top conducting layer is Silver (black lines) and photoconductive Silicon with $\sigma_{Si} = 1 \times 10^5$ S/m (red lines) to 1×10^3 S/m (green lines) and 2.5×10^{-4} S/m (blue lines), respectively. In the insets showing the designs yellow corresponds to metal (Silver) and grey corresponds to photoconductive Silicon.

Regarding the pure-metal (i.e. no Si) case, one can observe here the very large pure optical activity of both structures: of the inverse-cross structure at around 6 THz, and of the gammadion structure at around 3.5 THz. The large optical activity is associated in both cases with close to 80% transmittance.

Regarding the structures with incorporated Si, one should notice that, as in the structures presented in the previous sections, the highest achievable Si conductivity, i.e. 10^5 S/m, is not enough to reproduce the full metal case response. (This shows that the impressive polarization control capabilities of the full-metal case are almost exclusively a result of the coupling of the

#203516 - $15.00 USD Received 20 Dec 2013; revised 7 Mar 2014; accepted 23 Mar 2014; published 13 May 2014

two patterned metal plates of the unit cell.) Despite that, frequency regimes of significant tunable pure optical activity (i.e. optical activity associated with zero ellipticity) are observed in both structures (e.g. at ~9 THz for the cross-structure and at ~4 THz for the gammadion one), as well as switchable ellipticity response (e.g. around 7 THz for the crosses and 3 THz for the gammadion), indicating the merit of the structures for creating dynamic polarization control components.

5. Conclusions

We studied theoretically the dynamical tuning capabilities of different THz chiral metamaterial structures with specific metallic parts replaced by photoconducting silicon, which can be transformed from an insulating to an almost conducting state under proper photoexcitation. The circularly polarized transmission coefficients, the optical activity and the ellipticity of the transmitted wave have been calculated for different photoconductivities of Silicon, corresponding to various, practically achievable, photoexcitation intensities. The results show impressive dynamical tuning of the ellipticity of the transmitted wave, which does not vary monotonically with the Si photoconductivity. Quite significant tuning of the optical activity has been also observed in various frequency regimes. The prominent tuning capabilities of the proposed structures, along with their simplicity, which allows their easy fabrication and scaling towards optical frequencies, and the possibility to be fully flexible (since they are encapsulated in polyimide), makes them important candidate for the realization of active THz polarization manipulation components like polarization filters, modulators, wave-plates, etc.

Acknowledgments

This work was supported by Greek GSRT project ERC02-EXEL and by the EU-projects ENSEMBLE (grant no 213669) and By-Nanoera. Work at Ames Laboratory was partially supported by the Department of Energy (Basic Energy Sciences, Division of Materials Sciences and Engineering) under Contract No. DE-AC02-07CH11358 (computational studies). Author R. Z. acknowledges financial support by the Leverhulme Trust and the Royal Commission for the Exhibition of 1851 Research Fellowship in Science or Engineering. Author M. K. acknowledges useful discussions with Prof. Sergei Tretyakov.

#203516 - $15.00 USD Received 20 Dec 2013; revised 7 Mar 2014; accepted 23 Mar 2014; published 13 May 2014